

Academic City University College – Accra Ghana  
IEEE Area Six (6) Coordination Centre  
Tony Blair Institute for Global Change  
Trinity University, Lagos, Nigeria  
Harmarth Global Educational Services  
FAIR Forward – Artificial Intelligence for All  
Deutsche Gesellschaft für Internationale Zusammenarbeit (GIZ) GmbH  
Society for Multidisciplinary & Advanced Research Techniques (SMART)



---

---

Accra Bespoke Multidisciplinary Innovations Conference (ABMIC)

---

---

## Spectral Analyses Study of Boundary Layer Transition Delay with a Finite Compliant Panel

<sup>1</sup>Bori, I., <sup>2</sup>Yeo, K.S. & <sup>3</sup>Bako, S.

<sup>1</sup>Senior Lecturer, Dept of Mech. Engineering, Federal University of Technology, Minna, Nigeria

<sup>2</sup> Associate Professor, Department of Mechanical Engineering, National University of Singapore

<sup>3</sup> Lecturer, Department of Mechanical Engineering, Nuhu Bamali Polytechnic, Zaria, Nigeria

**Emails:** <sup>1</sup>ige.bori@futminna.edu.ng, <sup>2</sup>mpeyeoks@nus.edu.sg, <sup>3</sup>s2bako@yahoo.com

**Phones:** <sup>1</sup>+234 9032502267, <sup>2</sup>+65 6516-2246, <sup>3</sup>+234 8034503512

### ABSTRACT

Compliant panel or surface has been demonstrated in various theoretical investigations as a promising means in delaying transition further. Within the Blasius boundary layer, wavepackets were initiated at the flow upstream with a pulse-initiated disturbance, and this was allowed to evolve over a finite section of the wall that was replaced by a tensioned compliant panel (CP) on a damped foundation. In order to appreciate the work of the CP in transition delay, direct numerical simulation (DNS) was also carried on the rigid wall (RW) case for comparison purposes. Spectral (Double-Fourier transforms) analyses were performed on the obtained DNS data, and the results showed that, CP case was able to delay transition further, through the strategy of suppressing the linearly growing primary 2-D Tollmien-Schlichting (TS) waves mode, so that resultant wavepacket after the CP location was dominated by a pair of oblique waves. The practical implication of the obtained results show the possibility of drag force reduction over moving vehicles, which will translate to tangible economic gains for the total amount being spent on fuelling especially for those in transportation businesses.

**Keywords:** Compliant Panel, Wavepacket, Spectral Analyses

---

---

#### Proceedings Citation Format

Bori, I., Yeo, K.S. & Bako, S. (2022): Spectral Analyses Study of Boundary Layer Transition Delay with a Finite Compliant Panel. Proceedings of the 31<sup>st</sup> Accra Bespoke Multidisciplinary Innovations Conference. University of Ghana/Academic City University College, Accra, Ghana. 1<sup>st</sup> – 3<sup>rd</sup> June, 2022. Pp 7-16  
[www.isteams.net/ghanabespoke2022](http://www.isteams.net/ghanabespoke2022)  
[dx.doi.org/10.22624/AIMS/ABMIC2022P2](https://dx.doi.org/10.22624/AIMS/ABMIC2022P2)

---

---

## 1. INTRODUCTION

Studies on boundary layer transition is still an interesting one till now, because the state of the boundary layer whether laminar or turbulent, has a direct impact for instance on the drag force and heat transfer performance of many engineering devices. Practically, laminar state cannot be maintained for over a long period of time before turbulent state quickly set in, which is usually associated with much drag force. One of the possible ways to take an advantage of the laminar regime to a certain extent is to see how transition from the laminar state to the turbulent state could be effectively controlled or delayed further. Previous works in the literature had shown the successful applications of a compliant panel (a passive means), in delaying transition further within a boundary layer. It was considered as a special case of fluid-structure interaction problem; the classical theory of hydrodynamic stability over compliant surfaces has been remarked and classified as Time-Linearized Models (Dowel & Hall, 2001). Using this approach, many kinds of compliant wall models, including spring-backed membrane (Benjamin, 1963), bending plate (Carpenter & Garrad, 1985 and 1986) and volume-based viscoelastic layer (Willis, 1986), have been investigated and found to possess the potential for transition delay.

Merits of using compliant panel in delaying transition further includes: (i) it does not require any sophisticated control equipment or feedback system and (ii) also less expensive to implement compare with the active control type.

## 2. LITERATURE REVIEW

Laminar-turbulent transition problem started with the experiment of Reynolds (1883), followed by Prandtl (1904)'s work. An extension of that was applied to within the boundary layer which began with the theoretical computational works of Tollmien (1929) and Schlichting (1933) based on the Orr-Sommerfeld equation. More about boundary layer transitions and instabilities nature could be found in the paper published by Kachanov (2004). While in the numerical investigation realm, quite number of methods had been developed for investigating boundary-layer instability, transition and transition control. These methods include: Turbulence Modeling (TM) (Zhang et al. (1998)), Large Eddy Simulation (LES) (Ducros et al. (1996)), Linear Stability Theory (LST) (Reed et al (1996)), Parabolized Stability Equation (PSE) (Herbert (1997)) and Direct Numerical Simulation (DNS) (Kleiser & Zang (1991)). The first temporal direct numerical simulation of boundary-layer waves over a complaint surface (tensioned membrane to be specific) was performed by Domaradzki & Metacalfe (1987).

They studied the temporal and spatial behavior of the terms in the kinetic energy balance equation and verified the class A and class B character of the computed waves. Hall (1988) also developed a temporal simulation algorithm for simulating 2D instability waves over soft polyvinyl chloride (PVC) layers. Yeo & Dowling (1987) and Yeo (1990) also fully investigated the 2-D and 3-D linear stability of flows over isotropic and anisotropic viscoelastic coatings, including multi-layer coatings that are composed of several different layers of viscoelastic materials. Other recent works that involved wavepacket evolution within the boundary layer include: (i) for artificial disturbance in 2D and 3D (Yatskikh et al, 2020), (ii) supersonic boundary layer (Yermolaev et al, 2016), (iii) close to transonic speeds (Martinez et al, 2015), and (iv) to turbulent spots at high speeds (Polivanov et al, 2017).

### 3 NUMERICAL SIMULATIONS

#### 3.1 Numerical Scheme

The direct numerical simulation (DNS) code used by (Zhao, 2006) was further modified and used for these present simulations. The coupled fluid-wall dynamics is governed by the perturbation Navier-Stokes equations and compliant wall (surface-based model) equations:

$$\frac{\partial u_i}{\partial x_i} = 0, \quad (1)$$

$$\frac{\partial u_k}{\partial t} + \frac{\partial}{\partial x_i} (c_2 \bar{u}_i u_k + c_2 u_i \bar{u}_k + c_1 u_i u_k) = \frac{\partial}{\partial x_i} \left( \frac{1}{Re} \frac{\partial u_k}{\partial x_i} \right) - \frac{\partial p}{\partial x_k}, \quad (2)$$

Where

$i, k = 1, 2, 3$  represent the streamwise (x) the wall normal (y) and spanwise (z) coordinates of the Cartesian frame respectively.

The perturbation form of the Navier-Stokes equations (1) and (2) is obtained by letting  $c_1 = c_2 = 1.0$ , and  $\bar{u}_i$  represent the components of the base flow, where the base flow used in the present study is the non-parallel Blasius boundary layer profile. The numerical schemes and their associated discretization methods for equations (1) and (2) had already been described in detail by (Yeo et al, 2010). The Reynolds number  $Re$  is based on the free-stream velocity  $U_\infty$ . While the tensioned membrane (compliant panel) displacement is governed by equation (3):

$$m \frac{\partial^2 \eta}{\partial t^2} - T \left( \frac{\partial^2 \eta}{\partial x^2} + \frac{\partial^2 \eta}{\partial z^2} \right) + d \frac{\partial \eta}{\partial t} + k \eta = -p_w \quad (3)$$

where  $\eta$  represents the normal or y-displacement of the membrane surface.  $T$  represents the surface tension,  $m$  the mass per unit area of membrane,  $d$  is the damping coefficient, and  $k$  is the equivalent foundation elastic constant, and  $p_w$  as the external pressure acting on the compliant panel surface.

#### 3.2 Simulation Process And Computational Grids

For the sake of comparison, two independent studies were carried out namely: (i) Over a single compliant panel (CP) case and (ii) Over a rigid Wall (no embedded CP) case. The overall 3D view of the computational domain set-up is shown in figure 1, indicating the wavepacket generating (perturbation) source and the embedded compliant panel resting on a viscoelastic foundation, whose properties were designed to restrain the development of compliant-wall modes. Same 1D-springbacked tension compliant panel with damping has been used frequently in stability and transition delay investigations by many previous researchers. For over the single compliant panel case, computational domain used for the simulation spans  $310 \leq X \leq 1510$  in the streamwise (X) direction,  $0 \leq Y \leq 54$  in the wall normal (Y) direction and  $-172 \leq Z \leq 172$  in the spanwise (Z) direction, similar to what [11] used. A section of the rigid wall was replaced with finite length of a tensioned compliant panel from  $X = 450 - 762$  as shown in figure 2. That is, the panel was strategically placed in a region (just a few distances from the perturbation source) of the computational domain where the wavepacket will still be evolving in the linear regime, purposely to be able to suppress the developing 2D TS waves as soon as possible.

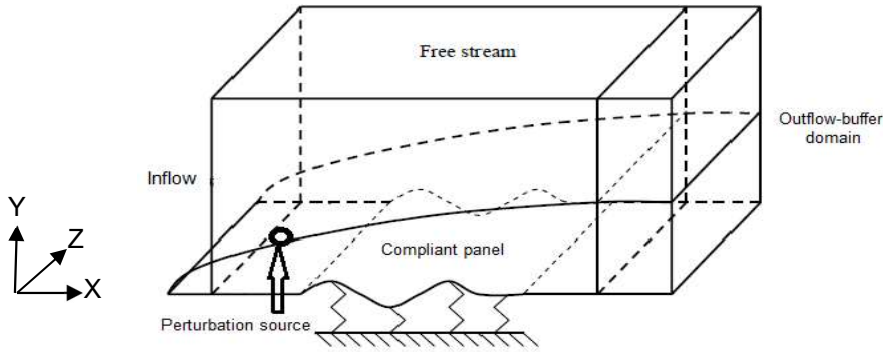


Fig. 1: 3D view of the computational domain

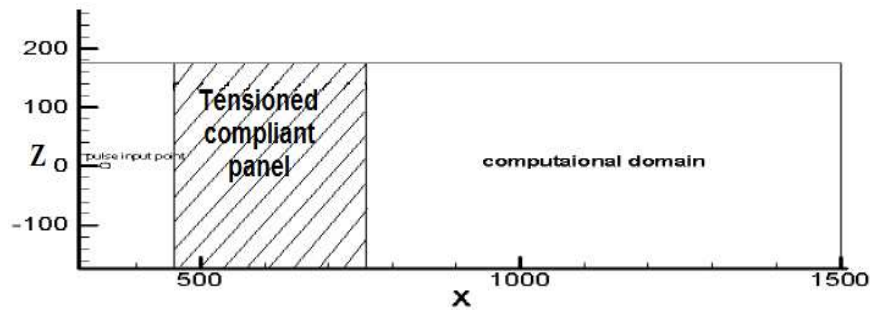


Fig. 2: Schematic plan views for the single-panel case

The  $(X, Y, Z)$  represents the non-dimensional Cartesian coordinates based on the reference length  $\delta_0$ , Where  $\delta_0 = 2.3182 \times 10^{-3} \text{ m}$  is the displacement thickness at the perturbation location. The number of grid points used in  $X, Y$  and  $Z$  directions are 1200, 85 and 195 respectively. Grid stretching was applied in the  $y$ -direction to ensure good and adequate resolution so as to capture fine flow details near the wall. The initiating pulse (perturbation) was introduced from the wall in a vertical ( $v$ -component) direction at the streamwise location  $X_0 = 349.4$  ( $x_0 = 81\text{cm}$ ). The free stream velocity is  $U_\infty = 6.65 \text{ m s}^{-1}$  and the kinematic viscosity is  $\nu = 1.49 \times 10^{-5} \text{ m}^2 \text{ s}^{-1}$ , and while the Reynolds number  $Re_\delta = \delta U_\infty / \nu$  at the excitation source is 1034.6. The non-dimensional simulation time  $T = tU_\infty / \delta_0$  is measured from the time of pulse initiation. The  $u$ -velocity component of the disturbance wavepacket were obtained at  $\frac{y}{\delta} \approx 0.62$ , similar to the heights at which wave measurements were made in the experiments of (Cohen et al, 1991) and (Medeiros & Gaster, 1999b).

### 3.3 Spectral Analyses

In order to properly understand the dynamics and the intrinsic phenomena involved as the wavepackets evolve from the point of perturbation until formation of turbulent spots is reached, spectrum analyses were carried out on the obtained simulation data. Double Fourier transforms of the flow quantities in time domain and sectional space domain were performed at selected non-dimensional heights  $y/\delta \approx 0.62$  and  $X$ -locations along the boundary layer. Also, in order to appreciate the positive contributions of the inserted finite length of the compliant panels, spectrum analysis results were compared with those for over the rigid wall case which were simulated under the same conditions.

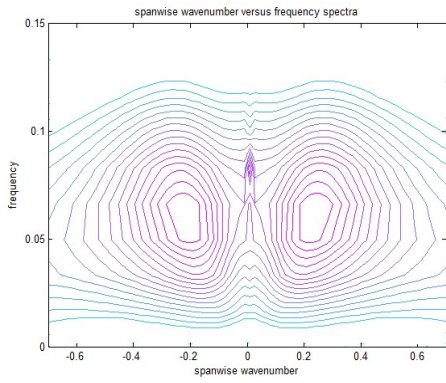
Nyquist criterion was duly observed during sampling and spectral data extracted such as wavepacket frequencies  $\omega$  and wavenumbers ( $\alpha$ ,  $\beta$ ) were converted to their local computational scale after the corresponding global quantities were obtained first. Also to add that, only streamwise ( $u$ ) velocity spectra are considered in this analysis being the flow field velocity component that contain the largest part of the wave energy.

#### 4. RESULTS AND DISCUSSION

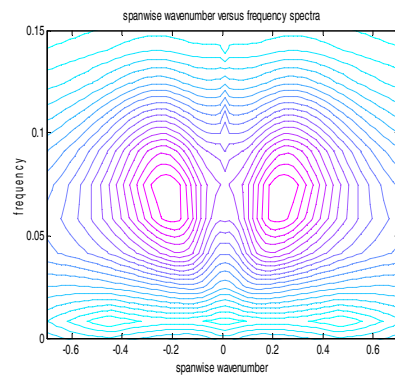
Figure 3 compares the  $u$ -velocity spectrum plots in terms of spanwise wavenumber  $\beta$  vs. frequency  $\omega$  plots between the rigid wall case (left column) and the single CP case (right column), in order to see clearly why the case with inserted CP did not breakdown quickly. Streamwise ( $X$ ) locations considered include before, during and after the single CP location so as to properly understand the overall spectral dynamics of the wavepackets. Figures 3(a1) and 3(a2) have almost the same spectral plots for both cases as the wavepacket is yet to reach the CP location for figure 3(a2). Figures 3(b2) and 3(c2)) are for when the wavepackets were directly traveling on top of the CP, and the interaction of the CP panel with the evolving wavepacket began to manifest itself as the spectral plots over this range differ from their counterparts for the rigid wall case. Distinct 2D and 3D mode waves peaks could be seen clearly in figures 3(b1) and 3(c1), whereas, it is difficult to see the distinct 2D and 3D mode wave peaks in figures 3(b2) and 3(c2), as everything looks mix-up, suggesting the strong interaction between the CP and the evolving wavepacket.

For figure 3(c2), the CP spectra of the wavepacket at this location shows weak low frequency 2D (spanwise wavenumber  $\beta \approx 0$ ) waves, which are absent for over the rigid wall spectral in figure 3(c1). These 2D or nearly 2D waves present in the wavepacket have something to do with its interaction with the compliant panel. It was noticed that the said low frequency 2D mode continue to die away as the wavepacket convects away from the compliant surface region. As the wavepacket convects further downstream, the dominant 2D wave modes continue to amplify over the rigid wall case in figure 3(d1) until it reaches a size (1.3%) that allows it to interact effectively with the accompanying oblique wave pair (which have also grown correspondingly) by the nonlinear instability mechanisms of (Herbert, 1988), leading to the accelerated growth of the oblique wave pair in figure 3(e1). From there onwards, further strong nonlinear interactions between the dominant oblique wave pair result in the development of low (near-zero) frequency waves for over the rigid wall wavepacket and the final breakdown of the rigid wall wavepacket in figure 3(f1). Whereas, over the compliant panel case in figure 3(f2) has not reached wavepacket breakdown stage yet, showing the embedded CP actually performed its work to a certain extent by delaying transition further.

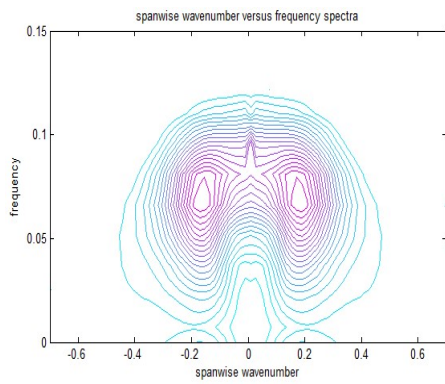
Also, the spectral properties for the dominant 2D and 3D wave modes were carefully extracted from the  $u$ -velocity spectral plot as already shown in figure 3. All data were extracted at height  $y/\delta(x) \approx 0.62$ . This was also repeated for over the rigid wall case just for the sake of comparison purpose. Figure 4 compares the spatial growth of the maximum disturbance  $u$ -velocity for both the RW and single CP cases in terms of 2D and 3D wave modes. 2D disturbance modes grow slower for the single CP case than its RW counterpart which is clearly seen at  $X = 1208$  in figure 4.



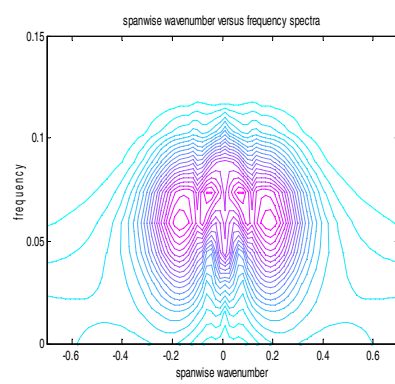
(a1)



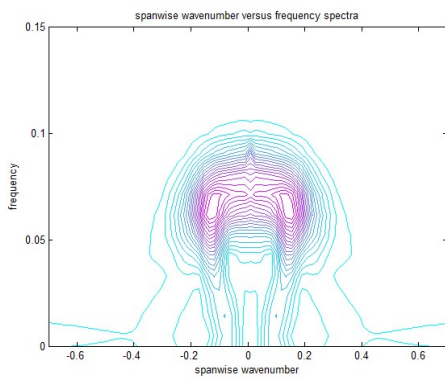
(a2)



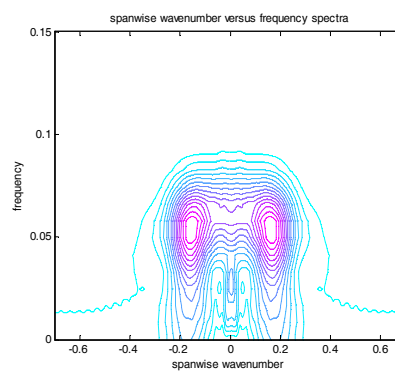
(b1)



(b2)



(c1)



(c2)

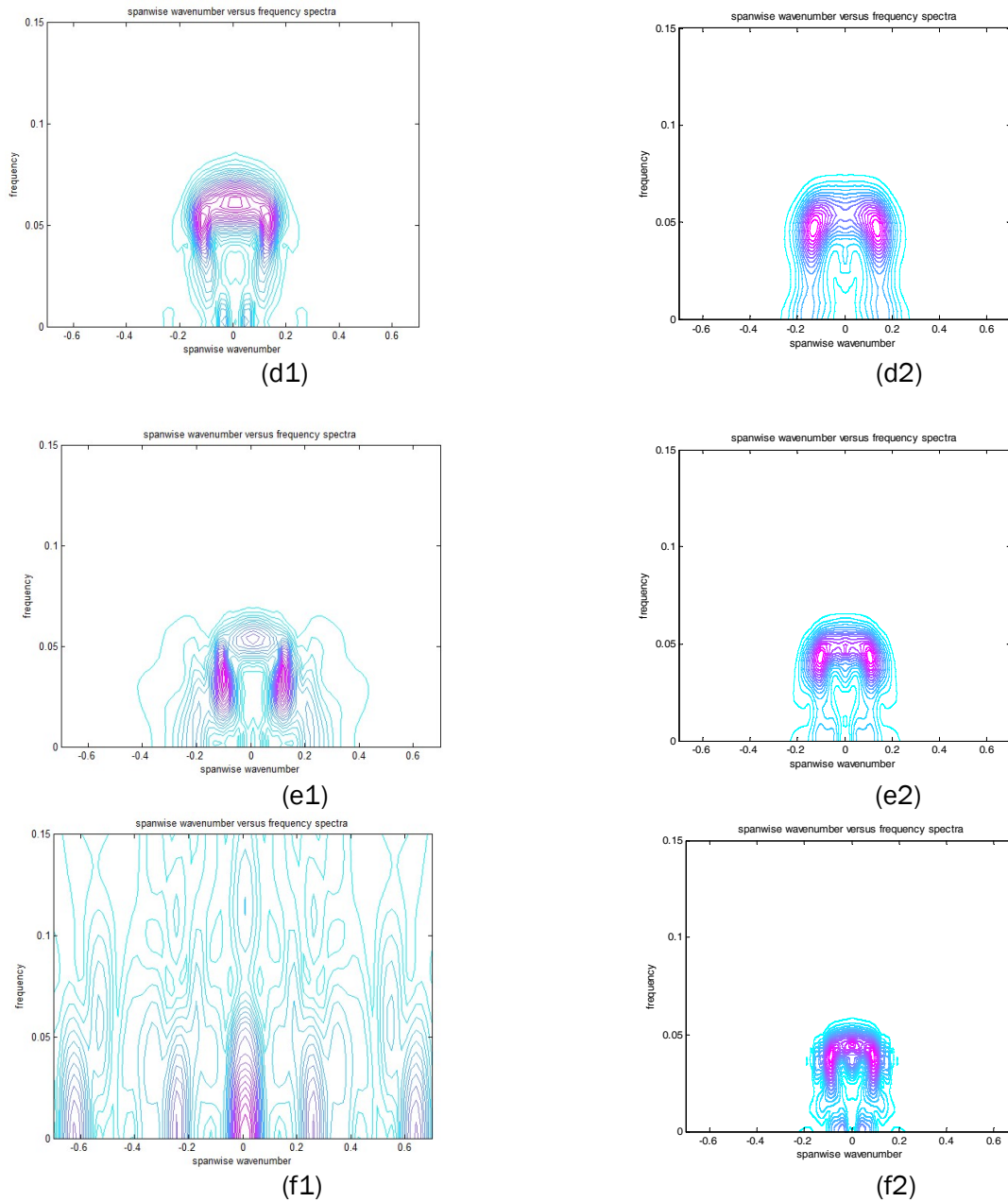


**Fig. 3: Comparison of spanwise wavenumber versus frequency spectra of streamwise u-velocity for different downstream locations at  $y/\delta \approx 0.62$  between rigid wall case (left column) and with compliant panel case (right column);  $\delta$  denotes the local displacement thickness. (a)  $X=392$  (b)  $X=518$ ; (c)  $X=690$ ; (d)  $X=949$ ; (e)  $X=1208$ ; (f)  $X=1467$ .**

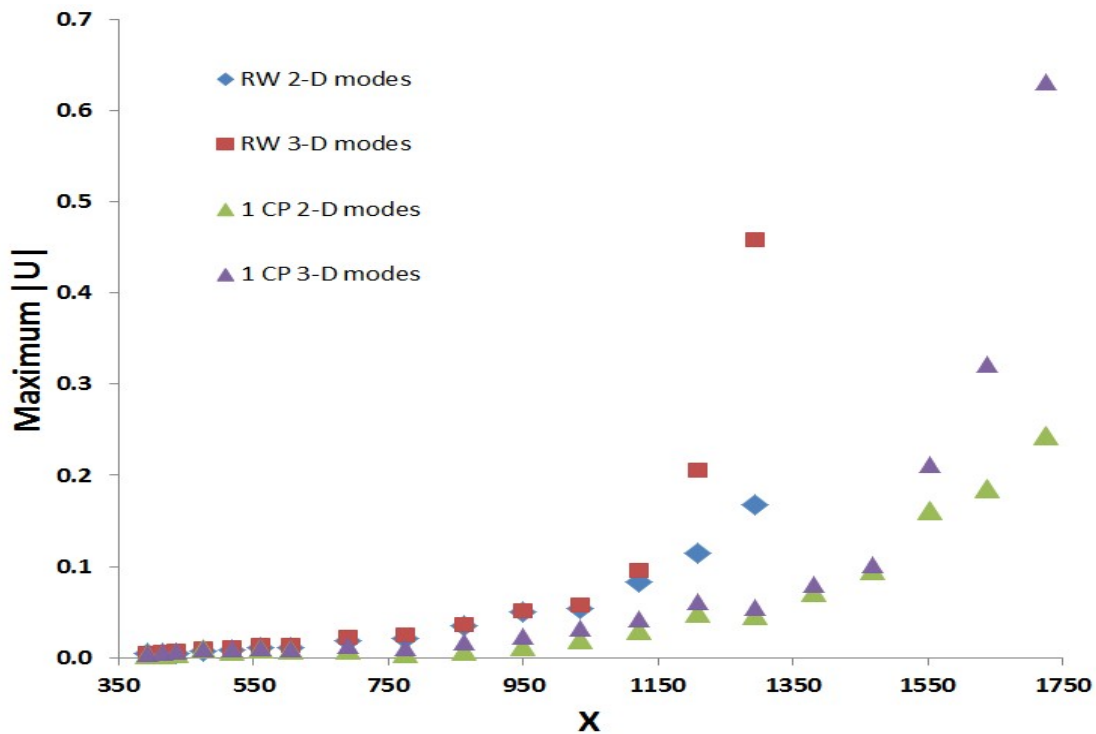


Fig. 4: Comparing the maximum wave growths between the Rigid wall (RW) and One CP cases

## 5. CONCLUDING REMARKS

Investigations on the use of short compliant panels to delay transition further within a Blasius boundary layer by DNS approach had been examined in this study. Small section of the rigid wall was replaced with a finite CP length from  $X = 450 - 762$  and this is dubbed the single CP case. Perturbation was carried out via introduction of vertical component ( $v$ ) velocity pulse at the flow upstream. A flexible compliant panel was carefully chosen with the aim to be able to stabilize Tollmien-Schlichting TS waves and same time help in delaying transition further. From the spectral analyses point of view, results for the single CP case show that the interaction of the compliant panel with the wavepacket when evolving over it caused suppression of 2-D wave modes. This confirms that the compliant panel is able to effectively attenuate the linearly growing primary 2-D TS wave mode, so that resultant wavepacket after the CP location was dominated by a pair of oblique waves. This study shows that attenuating the growth of the linearly evolving TS waves at its early stages and extending the linear regime correspondingly presents an effective strategy to delay transition further for the single CP case. In addition, the use of multiple compliant panels is recommended as future works, so as to ascertain if transition within the boundary layer could still be further delayed or not.

## REFERENCES

1. Dowell E.H. & Hall K.C., 2001, Modeling of fluid-structure interaction, Annual Review of Fluid Mechanics, vol.33, p.445.
2. Benjamin T.B., 1963, The three-fold classification of unstable disturbances in flexible surfaces bounding inviscid flows, Journal of Fluid Mechanics, vol. 16, p.436.
3. Carpenter P.W. & Garrad A.D., 1985, The hydrodynamic stability of flow over Kramer type compliant surfaces; Part 1 Tollmien-Schlichting Instabilities, J. Fluid Mech. 155, p. 465-510.
4. Carpenter P.W. & Garrad A.D., 1986, The hydrodynamic stability of flow over Kramer-type compliant surfaces. Part 2. Flow-induced surface instabilities, J. Fluid Mech. 170, p. 199-232.
5. Willis G .J. K., 1986, Hydrodynamic stability of boundary layers over compliant surfaces, PhD Thesis, Cambridge University, U.K, p. 243.
6. Reynolds O. 1883, On the experimental investigation of the circumstances which determine whether the motion water shall be direct or sinuous, and the law of resistance in parallel channels, Phil. Trans. Roy. Soc., vol. 174, pp. 935-982, 1183.
7. Prandtl L. Über Flüssigkeitsbewegung bei sehr kleiner Reibung, Verhandlg. III. Intern. Math. Kongr., Heidelberg, 1904, pp. 484-491.
8. Tollmien W., 1929, Über die entstehung der turbulenz, Nachr. Ges. Wiss. Göttingen, p.21-44.
9. Schlichting H., 1933, Zur entstehung der turbulenz bei der plattenströmung, Nachr. Ges.Wiss. Göttingen, p. 181-208.
10. Kachanov Y.S. 2004, Routes of boundary layer transition, IUTAM Symposium on one hundred years of boundary layer research, pp. 95-104.
11. Zhang X.Q., Liu C.Q., Liu F. & Yang C.I., 1998, Turbulent transition simulation using the k-omega model, International Journal for Numerical Methods in Engineering, vol.42, no.5, p.907.
12. Ducros F., Comte P. & Lesieur M., 1996, Large-eddy simulation of transition to turbulence in a boundary layer developing spatially over a flat plate, Journal of Fluid Mechanics, vol.326, p.1.
13. Reed H.L., Saric W.S. & Arnal D., 1996, Linear stability theory applied to boundary layers, Annual Review of Fluid Mechanics, vol.28, p.389.
14. Herbert T., 1997, Parabolized stability equations, Annual Review of Fluid Mechanics, vol.29, p.245.
15. Kleiser L. & Zang T.A., 1991, Numerical-simulation of transition in wall-bounded shear flows, Annual Review of Fluid Mechanics, vol.23, p.495.
16. Domaradzki J.A. & Metcalfe R.W., 1987, Stabilization of laminar boundary layers by compliant membranes, Physics of Fluids, vol.30 (3), p.695.
17. Hall M.S., 1988, The interaction between a compliant material and an unstable boundary layer flow, Journal of Computational Physics, vol.76, p.33.
18. Yeo K.S. & Dowling A.P., 1987, The stability of inviscid flow over passive compliant walls, Journal of Fluid Mechanics, vol. 183, p.265.
19. Yeo K.S., 1990, The hydrodynamic stability of boundary-layer flow over a class of anisotropic compliant walls, Journal of Fluid Mechanics, vol. 220, p.125.
20. Yatskikh A., Yermolaev Y., Kosinov A., Semionov N., and Semenov A. 2020. Evolution of localized artificial disturbance in 2D and 3D supersonic boundary layers.

21. Yermolaev Y.G., Yatskikh A.A. and Kosinov A.D. Wave analysis of the evolution of a single wave packet in supersonic boundary layer. In: 18th international conference on the methods of aerophysical research (ICMAR2016), Perm, Russia, 27 June -3 July 2016, paper no. 030037.
22. Martinez A.G., Gennaro E.M, and Medeiros M.A.F. Wavepackets in boundary layers close to transonic speeds. IUTAM\_ABCM Symposium on Laminar Turbulent Transition, Procedia IUTAM 14, 2015, pages 374 – 380.
23. P.A. Polivanov, Y.V. Gromiko, D.A. Bountin, A.A. Sidorenko, and A.A. Maslov, 2017. Evolution of a wavepacket to turbulent spot in a boundary layer at high speeds. Progress in Flight Physics 9, pages 435 – 450.
24. Zhao X., 2006, Computational simulation of wavepacket evolution over compliant surfaces, Ph.D. Thesis, National University of Singapore.
25. K.S. Yeo, X. Zhao, Z.Y. Wang and K.C. Ng, 2010, DNS of wavepacket evolution in a Blasius boundary layer. Journal of fluid mechanics, vol. 652, pp. 333-372.
26. Cohen J., Breuer K. S. & Haritonidis J. H., 1991, On the evolution of a wave packet in a laminar boundary layer, J. Fluid Mech. 225, p. 575-606.
27. Medeiros M.A.F & Gaster M., 1999b, The production of subharmonic waves in the nonlinear evolution of wavepackets in boundary layers, J. Fluid Mech. 399, p. 301-318.
28. Herbert T., 1988, Secondary instability of boundary layers, Ann. Rev. Fluid Mech.20, p.487-526.